

Superconductivity in graphene stacks: from the bilayer to graphite

Lizardo H. C. M. Nunes* and A. L. Mota
*Departamento de Ciências Naturais,
Universidade Federal de São João del Rei
36301-160 São João del Rei, MG, Brazil*

E. C. Marino
*Instituto de Física, Universidade Federal do Rio de Janeiro,
Cx. P. 68528, Rio de Janeiro-RJ 21941-972, Brazil*
(Dated: May 10, 2022)

We study the superconducting phase transition, both in a graphene bilayer and in graphite. For that purpose we derive the mean-field effective potential for a stack of graphene layers presenting hopping between adjacent sheets. For describing superconductivity, we assume there is an on-site attractive interaction between electrons and determine the superconducting critical temperature as a function of the chemical potential. This displays a dome-shaped curve, in agreement with previous results for two-dimensional Dirac fermions^{33,34}. We show that the hopping between adjacent layers increases the critical temperature for small values of the chemical potential. Finally, we consider a minimal model for graphite⁴¹ and show that the transition temperature is higher than that for the graphene bilayer for small values of chemical potential. This might explain why intrinsic superconductivity is observed in graphite.

PACS numbers: 74.25.Dw, 74.70.Wz

I. INTRODUCTION

Graphene is a one-atom-thick layer of graphite¹. The carbon atoms in each layer are arranged in a honeycomb lattice and the tight-binding energy presents a band structure such that the valence and conduction bands touch precisely in the vertices of two inequivalent Dirac cones in the Brillouin zone. The electronic excitations appearing in the conduction band have the dispersion relation of a relativistic massless particle and their properties, accordingly, will be determined by the Dirac equation. Graphene is believed to be the parent compound of most of the carbon-based systems and their electric, magnetic and elastic properties all originate from the properties of graphene.

Interestingly, several carbon-based compounds present superconductivity. For instance, the graphite intercalated compounds (GIC)² which consists of graphene sheets alternated by alkali layers, mainly acting as charge reservoirs, becomes superconducting with the transition temperature ranging from below 1K for KC_8 to 11.5 K for CaC_6 ³⁻⁶; some fullerides present critical temperatures as high as 33 K as applied pressure or the chemical composition increases the lattice parameter⁷; and there are reports of room temperature local superconductivity within isolated “grains” in highly oriented pyrolytic graphite (HOPG)⁸ and also with critical temperature $T_c \sim 25$ K in thin samples⁹. Moreover, a fully saturated hydrocarbon derived from a single graphene sheet, called graphane, is predicted to be a high-temperature electron-phonon superconductor exhibiting a critical temperature of above 90 K¹⁰.

Despite the fact that theoretical conjectures have been proposed as possible candidates to produce superconduc-

tivity¹¹⁻¹⁷, intrinsic superconductivity has never been observed in graphene, but it could be only induced by proximity effects, where a superconducting current propagated through a superconductor-normal-superconductor (SNS) Josephson junction, with graphene as the N region¹⁸.

Nevertheless, the stability of the superconducting phase has been investigated in graphene¹⁹⁻²¹ and the symmetry of the order parameter in the honeycomb lattice was identified; if there is an on-site net attractive interaction between electrons in the honeycomb lattice, the usual *s*-wave singlet pairing is favoured²². As nearest-neighbours attraction are taken into account, an exotic combination of *s*-wave and *p*-wave superconducting order parameters is possible²³. In the context of the *t*-*J*-*U* model, *f*-wave triplet-pairing and *d* + *id* singlet-pairing instabilities are found to emerge away from half-filling²¹.

Previously, some of us have investigated the phase diagram of a quasi-two-dimensional interacting Dirac electrons system forming Cooper pairs in the singlet state, which is a suitable model to describe a stack of uncoupled superconducting graphene sheets, and we have found a quantum critical point connecting the normal and superconducting phases at a certain critical coupling²⁴. If low magnetic fields are applied to the system, we have found a critical field as a function of the superconducting interaction²⁵.

In those previous investigations, the variation of the chemical potential was not taken into account; however, applying a bias voltage, the carrier density of graphene can be controlled by electric field effect. Therefore, in the present paper we investigate the effect of the chemical potential as a free parameter of our model and we also consider the effect of the out-of-plane hopping be-

tween adjacent graphene sheets. In order to describe graphite, we consider the minimal model with the electron tunneling between the nearest sites in the plane and out of the plane. We have found that the superconducting critical temperature is enhanced at small values of the chemical potential for graphite when compared to the values predicted by us for graphene bilayer, what might explain why intrinsic superconductivity has been observed in HOPG.

The paper is organized as follows: In Sec. II we present the model Hamiltonian for the graphene bilayer, the dispersion relation is calculated and the effective potential (free energy) is derived. In Sec. II A the superconducting phase diagram at $T = 0$ is obtained analyzing the minima conditions for the effective potential for several values of the interaction and the hopping between adjacent graphene sheets. In Sec. II B we calculate the superconducting critical temperature as a function of the chemical potential for several values of the hopping parameter between layers. The results represent an upper bound for the Kosterlitz-Thouless transition. In Sec. III our results for the superconducting phase diagram are extended for an infinite number of coupled graphene layers considering the electron tunneling amplitudes between the nearest sites in the plane and out of the plane. Sec. IV is devoted to the conclusion.

II. GRAPHENE BILAYER

Consider a stack of N graphene layers with a hopping term between adjacent planes, where the upper layer has its B sublattice on top of sublattice A of the underlying layer (Bernal stacking), as can be seen in Fig. 1. The Hamiltonian of each coupled layer is described by the following²⁶,

$$\begin{aligned} H_{t,l} = & -\mu \sum_{\mathbf{k},\sigma} \left[a_{\mathbf{k},\sigma,l}^\dagger a_{\mathbf{k},\sigma,l} + b_{\mathbf{k},\sigma,l}^\dagger b_{\mathbf{k},\sigma,l} \right] \\ & -t \sum_{\mathbf{k},\sigma} s_k \left[a_{\mathbf{k},\sigma,l}^\dagger b_{\mathbf{k},\sigma,l} + a_{\mathbf{k},\sigma,l+1}^\dagger b_{\mathbf{k},\sigma,l+1} \right] + \text{h.c.} \\ & -t_\perp \sum_{\mathbf{k},\sigma} a_{\mathbf{k},\sigma,l}^\dagger b_{\mathbf{k},\sigma,l+1} + \text{h.c.} , \end{aligned} \quad (1)$$

where the index $l = 1, \dots, N$ characterizes the different planes and μ is the chemical potential. The second line in the RHS of the above equation describes the hopping between electrons of different sublattices within a graphene sheet, while the third line describes the hopping between layers. The hopping parameter is about $t \approx 2.8$ eV and $t_\perp \approx t/10$. The operators $a_{i,\sigma,l}^\dagger = \sum_{\mathbf{k}} e^{i\mathbf{k}\cdot\mathbf{r}_i} a_{\mathbf{k},\sigma,l}^\dagger$ and $b_{i,\sigma,l}^\dagger = \sum_{\mathbf{k}} e^{i\mathbf{k}\cdot\mathbf{r}_i} b_{\mathbf{k},\sigma,l}^\dagger$ create, respectively, an electron on site i with spin σ on sublattice A and an electron on site i with spin σ on sublattice B of plane l . In the honeycomb lattice we have $s_k = 1 + e^{i\mathbf{k}\cdot\mathbf{a}_1} + e^{i\mathbf{k}\cdot\mathbf{a}_2}$, where $\mathbf{a}_1 = a\hat{e}_x$ and $2\mathbf{a}_2 = a(\hat{e}_x - \sqrt{3}\hat{e}_y)$, as shown in Fig. 1. The lattice parameter is $a = 2.46$ Å for graphene.

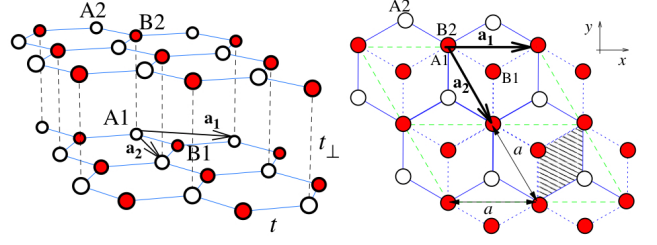


Figure 1: Lattice structure of two adjacent graphene layers (after²⁶).

We add an on-site attractive interaction between the electrons within each graphene layer forming Cooper pairs in the s -wave state. The interaction term is given by

$$\begin{aligned} H_{SC,l} = & -g \sum_{\mathbf{k},\mathbf{k}',\sigma} \left(a_{\mathbf{k},\sigma,l}^\dagger a_{-\mathbf{k},-\sigma,l}^\dagger a_{-\mathbf{k}',-\sigma,l} a_{\mathbf{k}',\sigma,l} \right. \\ & \left. + b_{\mathbf{k},\sigma,l}^\dagger b_{-\mathbf{k},-\sigma,l}^\dagger b_{-\mathbf{k}',-\sigma,l} b_{\mathbf{k}',\sigma,l} \right) , \end{aligned} \quad (2)$$

with $g > 0$. The origin of the interaction is to be determined by some underlying microscopic theory, which is not considered here. However, the symmetry of the gap originated from this interaction is consistent with the isotropic s -wave symmetry gap observed in some GICs²⁷.

Introducing the following Nambu fermion field,

$$\Psi_{\mathbf{k},l}^\dagger = \left(\psi_{\mathbf{k},l}^\dagger, \psi_{\mathbf{k},l+1}^\dagger \right) , \quad (3)$$

where

$$\psi_{\mathbf{k},l}^\dagger = \left(a_{\mathbf{k},\uparrow,l}^\dagger, b_{\mathbf{k},\uparrow,l}^\dagger, a_{-\mathbf{k},\downarrow,l}, b_{-\mathbf{k},\downarrow,l} \right) , \quad (4)$$

one can rewrite the combined Hamiltonian $H_{t,l} + H_{SC,l}$ at the mean-field level,

$$H_{\text{MF}} = \sum_{\mathbf{k}} \Psi_{\mathbf{k},l}^\dagger \mathcal{A} \Psi_{\mathbf{k},l} - \frac{\Delta\Delta^*}{g} \quad (5)$$

where, by definition, the superconducting order parameter is

$$-\frac{\Delta}{g} = \sum_{\mathbf{k}} \langle a_{\mathbf{k},\uparrow,l}^\dagger a_{-\mathbf{k},-\downarrow,l}^\dagger \rangle = \sum_{\mathbf{k}} \langle b_{\mathbf{k},\uparrow,l}^\dagger b_{-\mathbf{k},-\downarrow,l}^\dagger \rangle \quad (6)$$

and the 8×8 matrix \mathcal{A} in Eq. (5) is given by

$$\mathcal{A} = \begin{pmatrix} \mathcal{A}_1 & \mathcal{A}_{12} \\ \mathcal{A}_{21} & \mathcal{A}_2 \end{pmatrix} , \quad (7)$$

with

$$\mathcal{A}_1 = \mathcal{A}_2 = \begin{pmatrix} -\mu & -ts_k & 0 & \Delta \\ -ts_k^* & -\mu & \Delta & 0 \\ 0 & \Delta^* & \mu & ts_k^* \\ \Delta^* & 0 & ts_k & \mu \end{pmatrix} \quad (8)$$

and

$$\mathcal{A}_{12} = \mathcal{A}_{21}^T = \begin{pmatrix} 0 & -t_{\perp} & 0 & 0 \\ 0 & 0 & 0 & 0 \\ 0 & 0 & 0 & t_{\perp} \\ 0 & 0 & 0 & 0 \end{pmatrix}. \quad (9)$$

From H_{MF} in Eq. (5), follows the dispersion relation,

$$E_k = \pm \sqrt{|\Delta|^2 + E_{\text{BL}}^2}, \quad (10)$$

where

$$E_{\text{BL}} = \pm \sqrt{t^2 |s_{\mathbf{k}}|^2 + \left(\frac{t_{\perp}}{2}\right)^2} \pm \frac{t_{\perp}}{2} - \mu. \quad (11)$$

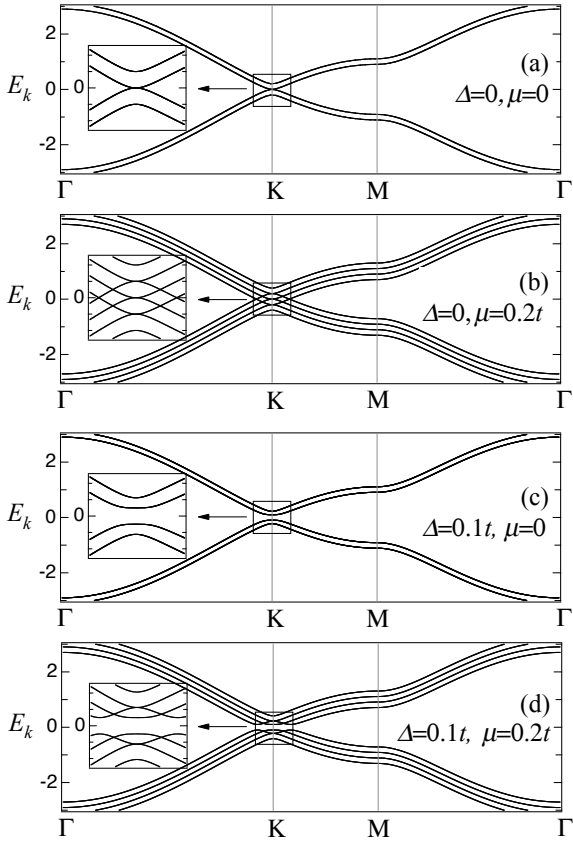


Figure 2: Band structure for (a) $\Delta = \mu = 0$, (b) $\Delta = 0$ and $\mu = 0.2t$, (c) $\Delta = 0.1t$ and $\mu = 0$ (d) $\Delta = 0.1t$ and $\mu = 0.2t$. Energy is given in units of t and $t_{\perp} = 0.2t$.

Let us neglect the hopping term between planes for a moment and consider only the normal state of the system at the Fermi level, which means $t_{\perp} = \Delta = \mu = 0$. In that case, \mathcal{A} has eight eigenvalues, but only two are undistinguished: $\pm t\sqrt{|s_{\mathbf{k}}|^2}$, which is exactly the dispersion relation of a single layer for a given spin state^{1,26}. For $\Delta \neq 0$, $\mu \neq 0$, we have $\pm\sqrt{|\Delta|^2 + (\mu \mp t|s_{\mathbf{k}}|)^2}$ for

each layer, which is the spectrum for the s -wave pairing²³.

If we take into account the hopping term between planes, in the absence of superconductivity, we obtain $\pm|E_{\text{BL}}|$. In particular, at $\mu = 0$, the four energy bands along three directions in the first Brillouin zone for $\Delta = \mu = 0$ can be seen in Fig. 2.a, which is the same plot shown for the unbiased graphene bilayer in²⁶. The eight distinct energy bands in the normal state are shown in Fig. 2.b. (It should be noticed that, for this particular choice of parameters, the chemical potential is sitting right at the bottom of the upper band.) As expected, the system is gapped in the superconducting state and the four energy bands at $\mu = 0$ are shown in Fig 2.c. Finally, the eight energy bands for nonzero gap and chemical potential are shown in Fig. 2.d.

The graphene dispersion relation has six Dirac points at the corners of the first Brillouin zone; however, only two of them are non-equivalent. The continuum limit of our model Hamiltonian is obtained expanding Eq. (5) in the vicinity of the Dirac points $\mathbf{K} = -4\pi/3a\hat{e}_x$ and $\mathbf{K}' = 4\pi/3a\hat{e}_x$,

$$H_{\text{MF},l}^{\text{CL}} = \sum_{\alpha} \int \frac{d^2k}{(2\pi)^2} \Psi_{\alpha,l}^{\dagger}(k) \mathcal{A}_{\alpha} \Psi_{\alpha,l}(k) - \frac{\Delta\Delta^*}{g}, \quad (12)$$

where $\alpha = K, K'$ and \mathcal{A}_{α} is obtained replacing $ts_{\mathbf{k}}$ by $-v_{\text{F}}(k_x - ik_y)$ and $-v_{\text{F}}(k_x + ik_y)$ in Eq.(8) for K and K' respectively, with $\hbar = 1$ and $v_{\text{F}} = \sqrt{3}ta/2$.

The partition function in the complex time representation is written as

$$\mathcal{Z} = \frac{1}{\mathcal{Z}_0} \int \mathcal{D}\Psi^* \mathcal{D}\Psi \exp \left\{ \sum_{l=1}^N \int_0^{\beta} d\tau L_{\text{MF},l}^{\text{CL}} \right\}, \quad (13)$$

where \mathcal{Z}_0 is the vacuum functional, $\beta = 1/k_{\text{B}}T$ (k_{B} is the Boltzmann constant) and

$$L_{\text{MF},l}^{\text{CL}} = \sum_{\alpha,\sigma} \int \frac{d^2k}{(2\pi)^2} \left(\psi_{\alpha,\sigma,l}^{\dagger} i\partial_{\tau} \psi_{\alpha,\sigma,l} - H_{\text{MF},l}^{\text{CL}} \right), \quad (14)$$

with $\psi_{\alpha,\sigma,l}^{\dagger} = [a_{\alpha,\sigma,l}^{\dagger}(k), b_{\alpha,\sigma,l}^{\dagger}(k)]$ representing the spinorial fields appearing in the continuum limit of the tight-binding graphene Hamiltonian density.

Integrating over the fermion fields, we get that the partition function is proportional to

$$\left(\frac{\det \mathcal{A}'_{\alpha,n}}{\det \mathcal{A}'_{\alpha,n}[\Delta = 0]} \right)^{2N}, \quad (15)$$

where $\mathcal{A}'_{\alpha,n} = -i\omega_n \mathbf{1} + \mathcal{A}_{\alpha}$ is a function of the Matsubara frequencies for fermions, $\omega_n = (2n + 1)\pi T$, and $\mathbf{1}$ is the 8×8 unity matrix, with $k_{\text{B}} = 1$ hereafter for the sake of simplicity.

Finally, redefining the coupling $g = \lambda/N$, the “effective

potential” per bilayer for each Dirac point will be

$$V_{\text{eff}} = 2 \frac{\Delta \Delta^*}{\lambda} - \frac{1}{\beta} \sum_n \left[\int \frac{d^2 k}{(2\pi)^2} \ln \left(\frac{\det \mathcal{A}'_{K,n}}{\det \mathcal{A}'_{K,n}[\Delta=0]} \right) \right]. \quad (16)$$

This would be the leading order in a $1/N$ expansion and would be the exact result for $N \rightarrow \infty$.

In the next section, we analyze the conditions for the appearance of superconductivity at zero temperature provided by our mean-field effective potential.

A. The superconducting instabilities at $T = 0$

We shall study the minima of the effective potential. The occurrence of superconductivity corresponds to the existence of nonzero solutions of the order parameter, which minimizes the effective potential.

Taking the derivative of V_{eff} with respect to the order parameter and summing over the Matsubara frequencies, we obtain

$$V'_{\text{eff}}(T) = \Delta^* \left[\frac{2}{\lambda} - \frac{1}{2} \sum_{j=1}^4 \int \frac{d^2 k}{(2\pi)^2} \frac{1}{\sqrt{|\Delta|^2 + \xi_j^2}} \tanh \left(\frac{\beta}{2} \sqrt{|\Delta|^2 + \xi_j^2} \right) \right], \quad (17)$$

where

$$\xi_j = \pm \sqrt{v_F^2 k^2 + \left(\frac{t_{\perp}}{2} \right)^2} \pm \frac{t_{\perp}}{2} - \mu. \quad (18)$$

The nonzero solutions for $|\Delta|$ are given equalizing to zero the expression within brackets in the Eq. (17) above, which provides a self-consistent gap equation. In particular, at zero temperature, we get

$$V'_{\text{eff}}(0) = \Delta^* \left[\frac{2}{\lambda} - \frac{1}{2} \sum_{j=1}^4 \int \frac{d^2 k}{(2\pi)^2} \frac{1}{\sqrt{|\Delta|^2 + \xi_j^2}} \right]. \quad (19)$$

Introducing a large momentum cutoff Λ/v_F , we can integrate Eq. (19) over k ,

$$V'_{\text{eff}} = \Delta^* \left\{ \frac{2}{\lambda} - \frac{1}{2\alpha} \sum_{a,b} \left[\sqrt{|\Delta|^2 + \xi_{ab}^2} - \sqrt{|\Delta|^2 + \epsilon_{ab}^2} \right] + \left(\mu - b \frac{t_{\perp}}{2} \right) \ln \left(\frac{\sqrt{|\Delta|^2 + \xi_{ab}^2} + \xi_{ab}}{\sqrt{|\Delta|^2 + \epsilon_{ab}^2} + \epsilon_{ab}} \right) \right\}, \quad (20)$$

where $\alpha = 2\pi v_F^2$, $a, b = \pm 1$,

$$\xi_{ab} = a \sqrt{\Lambda^2 + \left(\frac{t_{\perp}}{2} \right)^2} + b \frac{t_{\perp}}{2} - \mu, \quad (21)$$

and $\epsilon_{ab} = \xi_{ab}(\Lambda = 0)$.

In particular, for $\mu = t_{\perp} = 0$, the nonzero solutions for the superconducting gap are²⁴

$$\Delta = \frac{\alpha \lambda}{2} \left(\frac{\Lambda^2}{\alpha^2} - \frac{1}{\lambda^2} \right), \quad (22)$$

for $\lambda > \alpha/\Lambda$, what establishes quantum critical point for the onset of superconductivity in the system at the critical coupling $\lambda_c = \alpha/\Lambda$.

Evidencing Λ in (20), it can be reexpressed as

$$V'_{\text{eff}} = \frac{\Delta^*}{\tilde{\alpha}} \left\{ \frac{2}{\lambda'} - \frac{1}{2} \sum_{a,b} \left[\sqrt{|\tilde{\Delta}|^2 + \tilde{\xi}_{ab}^2} - \sqrt{|\tilde{\Delta}|^2 + \tilde{\epsilon}_{ab}^2} \right] + \left(\tilde{\mu} - b \frac{\tilde{t}_{\perp}}{2} \right) \ln \left(\frac{\sqrt{|\tilde{\Delta}|^2 + \tilde{\xi}_{ab}^2} + \tilde{\xi}_{ab}}{\sqrt{|\tilde{\Delta}|^2 + \tilde{\epsilon}_{ab}^2} + \tilde{\epsilon}_{ab}} \right) \right\}, \quad (23)$$

where $\lambda' = \lambda/\lambda_c$ and the tilde indicates that the quantity is divided by Λ . Since all the nonzero solutions for the gap are given by the expression between the curly brackets above, and given that it does not depend on any experimental data, our results are suitable to describe any planar Dirac fermion system with a hopping between adjacent sheets, assuming that Λ is the single free parameter of our model. Therefore, in the following we present our numerical results for Δ in terms of the parameter Λ .

Notice that the cutoff is always provided by the lattice in condensed matter systems. Indeed, we have $\Lambda = 2\pi \hbar v_F/a$ as an upper bound for the energy cutoff, and since a is the smallest distance scale, Λ becomes a natural high-energy cutoff. In fact, this frequently happens in condensed matter. A familiar example in the case of conventional, phonon mediated superconductivity, is the Debye frequency (energy) a natural cutoff that emerges in BCS theory. Moreover, we also constrain ourselves to positive values of the chemical potential up to $\mu/\Lambda = 0.9$, given the half bandwidth of Λ .

The case for $t_{\perp} = 0$ and finite μ with different values of interaction coupling has been exhaustively investigated by some of us²⁸. The plots of the superconducting gap as a function of μ for $\lambda/\lambda_c = 0.8$ are shown in Fig. 3. Starting at $\mu/\Lambda = 0$, the system is in the normal state, since $\lambda < \lambda_c$. As μ/Λ increases, Δ_0/Λ displays a dome-shaped plot: the system asymptotically becomes superconducting up to a maximum value at an optimal chemical potential and decreases as μ/Λ increases even further.

Notice that the system is not quantum critical but, in fact, the curve vanishes exponentially as $\mu \rightarrow 0$, hence, superconductivity persists down to $\mu = 0$.

Our results are consistent with²⁹, which also obtains a dome-shaped plot of Δ for relativistic interacting particles, as can be seen in Fig. 1 of their paper (choice of parameters I, referred as the *weak-coupling case*).

An interesting result is obtained as we increase the value of t_{\perp} , as can be seen in the inset of Fig. 3. For

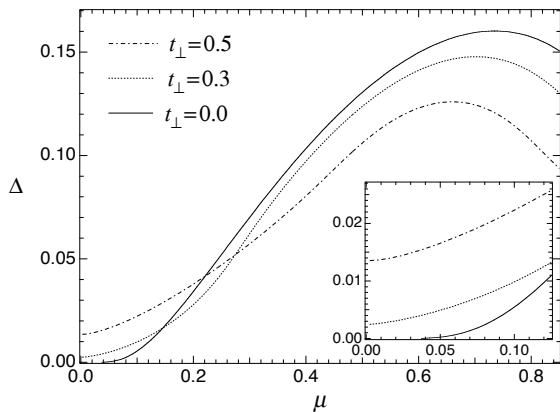


Figure 3: The superconducting gap as a function of the chemical potential for $t_{\perp} = 0, 0.3$ and 0.5 . The inset shows the same plot for a smaller range of the chemical potential. $\lambda/\lambda_c = 0.8$ and all the other quantities are given in unities of Λ .

small values of the chemical potential, as the out of the plane hopping between layers increases, we see that the superconducting gap also increases for the same value of the chemical potential. Indeed, even for $\mu = 0$, for which there is no superconducting gap when $t_{\perp} = 0$, given that $\lambda < \lambda_c$, there is a nonzero value of Δ for $t_{\perp}/\Lambda = 0.3$ or 0.5 , indicating that the system is in the superconducting state. Therefore, the hopping between layers favors the appearance of superconductivity.

As shall be seen in the next section, since the energy gap and the superconducting critical temperature tend to be proportional quantities, this result also shows that the superconducting critical temperature increases as the hopping between layers increases for small values of the chemical potential.

B. Superconducting phase at finite temperatures

In this section we calculate the superconducting phase diagram for finite temperatures. *A priori*, the nonzero solutions for Δ are supposed to hold only in the $N \rightarrow \infty$ limit at a finite temperature, because, otherwise, they are ruled out by the Coleman-Mermin-Wagner-Hohenberg theorem³⁰. This limit corresponds to a physical situation where the three-dimensionality of the system is explicitly taken into account. For finite values of N and $T \neq 0$, there is an underlying Berezinskii-Kosterlitz-Thouless (BKT) transition³¹, below which phase coherence is found for a nonzero Δ . The actual superconducting transition occurs at $T_{BKT} \leq T_c$. However, it can be shown that $T_{BKT} \xrightarrow{N \rightarrow \infty} T_c$ ³². This clearly indicates that, in spite of the fact that we may have a nonzero superconducting gap at $T = T_c$, only in a really three-dimensional system we will have phase coherence developing at the same temperature that the modulus of the order parameter

becomes nonzero, as determined by the gap equation. Therefore, T_c calculated in this section may be regarded as a mean-field upper bound critical temperature for the KT transition, which sets the actual temperature for the appearance of superconductivity in the $N \rightarrow \infty$ limit.

We start considering the gap equation provided by the Eq. (17). Making the change of variables $x = (v_F k)^2$, we get

$$\frac{1}{\lambda} - \frac{1}{8\alpha} \sum_{a,b} \int_0^{\Lambda^2} dx \frac{1}{E_{ab}(x)} \tanh \left[\frac{E_{ab}(x)}{2T} \right] = 0, \quad (24)$$

where

$$E_{ab}(x) \equiv \sqrt{|\Delta|^2 + \xi_{ab}^2(x)}, \quad (25)$$

with $\xi_{ab}(x)$ given by Eq. (21), replacing Λ^2 for x . From Eq. (24), we calculate the superconducting critical temperature T_c making $\Delta = 0$ at $T = T_c$ in the above expression.

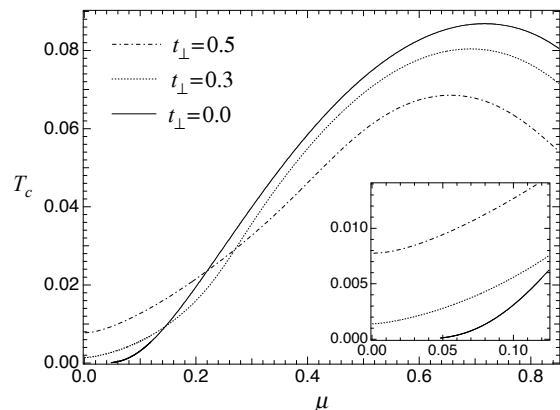


Figure 4: The superconducting critical temperature as a function of the chemical potential for $t_{\perp} = 0, 0.3$ and 0.5 . The inset shows the same plot for a smaller range of the chemical potential. $\lambda/\lambda_c = 0.8$ and all the other quantities are given in unities of Λ .

In Section II A we have found a dome-shaped superconducting gap as a function of the chemical potential for $\lambda < 1$ and several values of t_{\perp} . Since the energy gap and the superconducting critical temperature T_c are proportional, we expect to find a dome-shaped plot for T_c as a function of μ as well. In fact, as can be seen in Fig. 4, our numerical results for the superconducting critical temperature presents the characteristic dome experimentally observed in several compounds, like 1111 pnictides and cuprate superconductors.

A dome-like structure of the superconducting phase for two-dimensional Dirac fermions has been previously obtained in³³, where the superconducting critical temperature also presents a dome at intermediate filling fractions, surrounded by the normal phase for fillings close to unity or zero, which is consistent to our results. Also, a

dome for T_c as a function of hole concentrations has been previously obtained in a brief letter by some of us³⁴ for a relativistic version of the spin-fermion Hamiltonian³⁵, used to describe the Cu-O planes in the cuprates. Those results and the phase diagram presently calculated suggest that Dirac fermions may play a relevant role in the description of cuprates and iron pnictides.

Indeed, it has been shown that Dirac points appear in the intersection of the nodes of the d-wave superconducting gap and the 2D-Fermi surface in the high- T_c cuprate superconductors and the low-energy excitations will correspond exclusively to these points³⁶. Also, it has been experimentally found that the iron pnictides^{37,38} also present electronic excitations whose properties are governed by the Dirac equation. Theoretical results also support the existence of Dirac electrons in the pnictides^{39,40}.

As also suggested in the former section, the inset of Fig. 3 shows that, for a small value of μ , T_c increases as the t_\perp parameter is increased, indicating that the hopping between layers favors the appearance of superconductivity in the system.

As shall be seen in the next section, the same feature is observed as we take into account the first-neighbors out of the plane hopping between adjacent layers, which is the case for graphite.

III. GRAPHITE

In this section, we calculate the superconducting phase diagram of many coupled graphene layers for a finite chemical potential. To simplify the problem, we consider only the minimal model where only the electron tunneling amplitudes between the nearest sites in the plane t and out of the plane t_\perp are regarded. The same approach was employed in⁴¹, as briefly explained below.

Consider a Bernal-stacked graphene bilayer described by the following Hamiltonian in the vicinity of each non-equivalent Dirac point²⁶,

$$H_{\text{BL}} = \sum_{\mathbf{k}, \sigma} \Phi_{\mathbf{k}, \sigma}^\dagger \mathcal{B}_{\mathbf{k}} \Phi_{\mathbf{k}, \sigma}, \quad (26)$$

where the above 4×4 matrix $\mathcal{B}_{\mathbf{k}}$ is given by

$$\mathcal{B}_{\mathbf{k}} = \begin{pmatrix} v_F \mathbf{k} \cdot \vec{\sigma} & \mathcal{B}_{12} \\ \mathcal{B}_{21} & v_F \mathbf{k} \cdot \vec{\sigma} \end{pmatrix}, \quad (27)$$

the vector $\vec{\sigma} = (\sigma_x, \sigma_y)$ is written in terms of the well-known Pauli matrices, the matrix \mathcal{B}_{12} is

$$\mathcal{B}_{12} = \mathcal{B}_{21}^T = \begin{pmatrix} 0 & t_\perp \\ 0 & 0 \end{pmatrix}, \quad (28)$$

and $\Phi_{\mathbf{k}, \sigma}^\dagger = (\phi_{\mathbf{k}, \sigma, 1}^\dagger, \phi_{\mathbf{k}, \sigma, 2}^\dagger)$, with $\phi_{\mathbf{k}, \sigma, j}^\dagger = (a_{\mathbf{k}, \sigma, j}^\dagger, b_{\mathbf{k}, \sigma, j}^\dagger)$, $j = 1, 2$ denotes the layer index.

The model Hamiltonian for graphite is assumed to be described as an infinite number of graphene layers coupled by the hopping between adjacent sheets. Therefore,

introducing the operator

$$\tilde{\Phi}_{\mathbf{k}, \sigma}^\dagger = \left(\cdots \phi_{\mathbf{k}, \sigma, l-1}^\dagger \phi_{\mathbf{k}, \sigma, l}^\dagger \phi_{\mathbf{k}, \sigma, l+1}^\dagger \cdots \right), \quad (29)$$

the Hamiltonian becomes

$$H_{\text{Gr}} = \sum_{\mathbf{k}, \sigma} \tilde{\Phi}_{\mathbf{k}, \sigma}^\dagger \mathcal{C}_{\mathbf{k}} \tilde{\Phi}_{\mathbf{k}, \sigma}, \quad (30)$$

where

$$\mathcal{C}_{\mathbf{k}} = \begin{pmatrix} \ddots & & & & & & \\ & v_F \mathbf{k} \cdot \vec{\sigma} & \mathcal{B}_{12} & & & & \\ & \mathcal{B}_{21} & v_F \mathbf{k} \cdot \vec{\sigma} & \mathcal{B}_{12} & & & \\ & & \mathcal{B}_{21} & v_F \mathbf{k} \cdot \vec{\sigma} & & & \\ & & & & \ddots & & \\ & & & & & & \ddots \end{pmatrix}. \quad (31)$$

Introducing the momentum k_z in the z direction, it is possible to re-express the Hamiltonian for graphite taking the first-neighbors hopping between adjacent layers in the momentum representation, which is written in terms of a 4×4 matrix similar to $\mathcal{B}_{\mathbf{k}}$ in Eq. (27)⁴¹,

$$H_{\text{Gr}} = \sum_{\mathbf{k}, k_z, \sigma} \Phi_{\mathbf{k}, k_z, \sigma}^\dagger \mathcal{D}_{\mathbf{k}, k_z} \Phi_{\mathbf{k}, k_z, \sigma}, \quad (32)$$

where

$$\mathcal{D}_{\mathbf{k}, k_z} = \begin{pmatrix} v_F \mathbf{k} \cdot \vec{\sigma} & 2 \mathcal{B}_{12} \cos k_z d \\ 2 \mathcal{B}_{21} \cos k_z d & v_F \mathbf{k} \cdot \vec{\sigma} \end{pmatrix}, \quad (33)$$

and d is the distance between layers.

For this minimal model, the dispersion relation is given by

$$E_{\text{Gr}} = \pm \sqrt{|v_F \mathbf{k}|^2 + (t_\perp \cos k_z d)^2} \pm t_\perp \cos k_z d \quad (34)$$

and, for $k_z d = \pi/2$, we recover the Dirac-type dispersion found in graphene.

Taking into account the attractive interaction forming Cooper pairs within each graphene layer, as seen in Eq. (2), and introducing the operator

$$\tilde{\Psi}_{\mathbf{k}, \sigma}^\dagger = \left(\cdots \psi_{\mathbf{k}, \sigma, l-1}^\dagger \psi_{\mathbf{k}, \sigma, l}^\dagger \psi_{\mathbf{k}, \sigma, l+1}^\dagger \cdots \right), \quad (35)$$

where $\psi_{\mathbf{k}, \sigma, l}^\dagger$ is given by Eq. (4), the model Hamiltonian which describes the superconducting graphite in a mean-field approximation becomes

$$H_{\text{Gr, SC}} = \sum_{\mathbf{k}, \sigma} \tilde{\Psi}_{\mathbf{k}, \sigma}^\dagger \mathcal{E}_{\mathbf{k}} \tilde{\Psi}_{\mathbf{k}, \sigma}, \quad (36)$$

where

$$\mathcal{E}_{\mathbf{k}} = \begin{pmatrix} \ddots & & & & & & \\ & \mathcal{A}_1 & \mathcal{A}_{12} & & & & \\ & \mathcal{A}_{21} & \mathcal{A}_2 & \mathcal{A}_{12} & & & \\ & & \mathcal{A}_{21} & \mathcal{A}_1 & & & \\ & & & & \ddots & & \\ & & & & & & \ddots \end{pmatrix}, \quad (37)$$

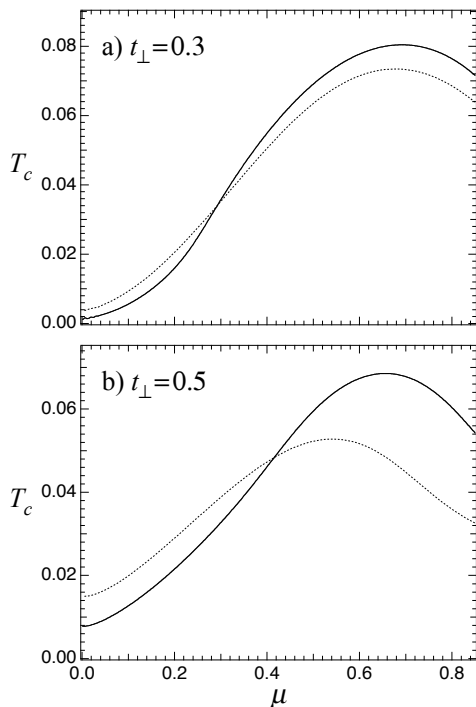


Figure 5: The superconducting critical temperature as a function of the chemical potential for (a) $t_{\perp} = 0.3$ and (b) $t_{\perp} = 0.5$ for both graphene bilayer (solid line) and graphite (dotted line). The inset in each pane shows the same plot for a smaller range of the chemical potential. $\lambda/\lambda_c = 0.8$ and all the other quantities are given in unities of Λ .

with $\mathcal{A}_1 = \mathcal{A}_2$ and $\mathcal{A}_{12} = \mathcal{A}_{21}^T$ given by the Eqs. (8) and (9) respectively.

Accordingly, it is possible to re-express the Hamiltonian for the superconducting graphite in terms of an 8×8 matrix, which is similar to $\mathcal{A}_{\mathbf{k}}$ in Eq. (7),

$$H_{\text{Gr,SC}} = \sum_{\mathbf{k}, k_z, \sigma} \Psi_{\mathbf{k}, k_z, \sigma}^{\dagger} \mathcal{F}_{\mathbf{k}, k_z} \Psi_{\mathbf{k}, k_z, \sigma}, \quad (38)$$

where

$$\mathcal{F}_{\mathbf{k}, k_z} = \begin{pmatrix} \mathcal{A}_1 & 2\mathcal{A}_{12} \cos k_z d \\ 2\mathcal{A}_{21} \cos k_z d & \mathcal{A}_2 \end{pmatrix} \quad (39)$$

and the dispersion is given by the 8 eigenvalues

$$E_{\pm}(\mathbf{k}, k_z) = \pm \sqrt{|\Delta|^2 + (E_{\text{Gr}} - \mu)^2}, \quad (40)$$

with E_{Gr} given by Eq. (34).

Therefore, the self-consistent equation for the superconducting gap becomes

$$\frac{2}{\lambda} = \frac{1}{2} \sum_{j=1}^4 \int_{-\frac{\pi}{2}}^{\frac{\pi}{2}} \frac{dk_z}{2\pi d} \int \frac{d^2 k}{(2\pi)^2} \frac{1}{E_+(\mathbf{k}, k_z)} \tanh \left[\frac{\beta}{2} E_+(\mathbf{k}, k_z) \right], \quad (41)$$

where the four values of $E_+(\mathbf{k}, k_z)$, labeled by the index j in the above expression, are given by E_{Gr} in Eq. (34), in analogy to the discussions in the previous sections.

We calculate the critical temperature from Eq. (41) and our results are compared with T_c obtained for graphene bilayer, from the former section. Our results are shown in Fig. 5 and we see that there is not an enhancement of T_c for every range of chemical potential for a given value of t_{\perp} . However, given t_{\perp} , we always find that the critical temperature for graphite is bigger than the T_c obtained for graphene bilayer for small values of the chemical potential, what demonstrates that the first neighbors hopping between adjacent sheets favors the superconductivity in the system.

IV. CONCLUSIONS

In conclusion, in the present paper we have derived the effective potential for a stack of graphene layers with a hopping between adjacent sheets and an on-site attractive interaction between electrons in a mean-field approximation.

For a single layer or two adjacent coupled layers of graphene, a remarkable result was obtained for the superconducting critical temperature as a function of the chemical potential: it displays a dome-shaped curve, as experimentally observed in several compounds, like 1111 pnictides and cuprate superconductors. This result suggests that Dirac fermions may play a relevant role in the description of cuprates and iron pnictides, which shall be object of further investigation. Indeed, a dome-like structure of the superconducting phase is in agreement with previous results for strongly interacting two-dimensional Dirac fermions^{33,34}. As pointed out in³³, our results can also be experimentally realized with ultracold atoms in a two-dimensional optical square lattice.

Finally, considering a minimal model for graphite, taking into account only the tunneling amplitudes between the nearest sites in the plane and out of the plane⁴¹, we have compared the superconducting critical temperature for graphite and graphene bilayer. We have seen that the T_c calculated for graphite is bigger than the one for graphene bilayer for a small value of μ , what might explain why intrinsic superconductivity is observed in HOPG.

Acknowledgments

This work has been supported in part by CNPq, FAPEMIG and FAPERJ. We would like to thank N. M. R. Peres, H. Caldas, and A. H. Castro Neto for discussions on related matters.

-
- * Electronic address: lizardonunes@ufsj.edu.br
- ¹ A. H. Castro Neto et al., Rev. Mod. Phys. **81**, 109 (2009).
 - ² Csányi G et al., Nat. Phys. **1**, 42 (2005).
 - ³ T. E. Weller et al., Nat. Phys. **1**, 39 (2005).
 - ⁴ N. Emery et al. Phys. Rev. Lett. **95**, 087003 (2005).
 - ⁵ I. T. Belash et al., Synt. Metals **36**, 283 (2002).
 - ⁶ N. B. Hannay et al., Phys. Rev. Lett. **14**, 225 (1965).
 - ⁷ O. Gunnarsson, Rev. Mod. Phys. **69**, 575 (1997).
 - ⁸ Y. Kopolevich, J. Low Temp. Phys. **119**, 691 (2000); Y. Kopelevich et al., Physics of the Solid State **41**, 1959 (1999) [Fizika Tverd. Tela (St. Petersburg) **41** (1999) 2135].
 - ⁹ P. Esquinazi et al., Phys. Rev. B **78**, 134516 (2008).
 - ¹⁰ G. Savini, A. C. Ferrari and F. Giustino Phys. Rev. Lett. **105**, 037002 (2010).
 - ¹¹ Z. Y. Meng et al., Nature **464**, 847 (2010).
 - ¹² S. Pathak, V. B. Shenoy and G. Baskaran Phys. Rev. B **81**, 085431 (2010).
 - ¹³ N. B. Kopnin and E. B. Sonin, Phys. Rev. Lett. **100**, 246808 (2008).
 - ¹⁴ G. Baskaran Phys. Rev. B **65**, 212505 (2002).
 - ¹⁵ Y. Jiang et al., Phys. Rev. B **77**, 235420 (2008).
 - ¹⁶ A. M. Black-Schaffer and S. Doniach, Phys. Rev. B **75**, 134512 (2007).
 - ¹⁷ B. Roy B and I. F. Herbut Phys. Rev. B **82**, 035429 (2010).
 - ¹⁸ H. B. Heersche, P. Jarillo-Herrero, J. B. Oostinga, L. M. K. Vandersypen, and A. F. Morpurgo, Nature **446**, 56 (2007).
 - ¹⁹ F. M. D. Pellegrino, G. G. N. Angilella and R. Pucci, Eur. Phys. J. B **76**, 469 (2010).
 - ²⁰ D. V. Khveshchenko, J. Phys.: Condens. Matter **21**, 075303 (2009).
 - ²¹ C. Honerkamp, Phys. Rev. Lett. **100**, 146404 (2008).
 - ²² E. Zhao and A. Paramekanti, Phys. Rev. Lett. **97**, 230404 (2007).
 - ²³ B. Uchoa B and A. H. Castro Neto, Phys. Rev. Lett. **98**, 146801 (2007).
 - ²⁴ E. C. Marino and L. H. C. M. Nunes Nuc. Phys. B **741** [FS] 404 (2006).
 - ²⁵ E. C. Marino and L. H. C. M. Nunes Nuc. Phys. B **769** [FS] 275 (2007).
 - ²⁶ Eduardo V. Castro et al., An Introduction to the Physics of Graphene Layers, in *Strongly Correlated Systems, Coherence and Entanglement*, (World Scientific, 2007)
 - ²⁷ R. K. Kremer, J. S. Kim and A. Simon Carbon Based Superconductors, in *High Tc Superconductors and Related Transition Metal Oxides*, (Springer-Verlag, Berlin Heidelberg, 2007)
 - ²⁸ L. H. C. M. Nunes, R. L. S. Farias. E. C. Marino, *Superconducting and excitonic quantum phase transitions in doped systems with Dirac electrons ref do cond-mat*
 - ²⁹ K. Fukushima and K. Iida, Phys. Rev. D **76**, 054004 (2007).
 - ³⁰ N. D. Mermin and H. Wagner, Phys. Rev. Lett. **17**, 1133 (1966); P. C. Hohenberg, Phys. Rev. **158**, 383 (1967); S. Coleman, Commun. Math. Phys. **31**, 259 (1973).
 - ³¹ V.L.Berezinskii, Zh. Eksp. Teor. Fiz. **59**, 907 (1970); J.Kosterlitz and D.Thouless, J. Phys. C **6**, 1181 (1973).
 - ³² E. Babaev, Phys. Lett. B **497**, 323 (2001).
 - ³³ L.-K. Lim et al., Eur. Phys. Lett. **88**, 36001 (2009).
 - ³⁴ L. H. C. M. Nunes and E. C. Marino, Physica B **378-380**, 704 (2006).
 - ³⁵ A.P. Kampf, Phys. Rep. **249**, 219 (1994).
 - ³⁶ I. Affleck and J. B. Marston Phys. Rev. B **37**, 3774 (1988); Phys. Rev. B **39**, 11 538 (1989); X-G. Wen and P. A. Lee Phys. Rev. Lett. **76**, 503 (1996).
 - ³⁷ Y. Kamihara et al., J. Am. Chem. Soc. **130**, 3296 (2008).
 - ³⁸ M. Rotter, M. Tegel M and D. Johrendt, Phys. Rev. Lett. **101**, 107006 (2008).
 - ³⁹ P. Richard et al., Phys. Rev. Lett. **104**, 137001 (2010).
 - ⁴⁰ C. M. S. da Conceição, M. B. Silva Neto and E. C. Marino, Phys. Rev. Lett. **106**, 117002 (2011).
 - ⁴¹ S. S. Pershoguba and V. M. Yakovenko, Phys. Rev. B **82**, 205408 (2010).